Bringing the lab to the fab: Robot-based inline measurement system for precise 3D surface inspection in vibrational environments

Daniel Wertjanz, Ernst Csencsics, Thomas Kern, and Georg Schitter, *Senior Membership, IEEE*

***Abstract*—This paper presents the integrated design of a robot-based inline measurement system for precise 3D surface inspection on free-formed objects. The measurement system comprises a MAGLEV measurement platform that is mounted to an industrial robot and enables the out-of-plane tracking of an arbitrarily oriented sample surface. This establishes lab-like conditions for the integrated optical 3D measurement tool directly in a vibrational environment. Using a PID control architecture with a tracking control bandwidth of 600 Hz, the effects of a vibration signal with 15.5 µm rms can be reduced to disturbances with 236 nm rms. The orientation-independent measurement performance is demonstrated by imaging a calibration standard with 20 µm pitch in various robot poses. Experiments show that the system is capable of reducing the axial measurement uncertainty by a factor of 12, enabling robot-based 3D measurements with sub-micrometer resolution on freeform surfaces in a vibrational environment.**

***Index Terms*—Mechatronics, System integration, Vibration control.**

I. Introduction

INDUSTRIAL high-tech manufacturing systems are facing a continuously growing demand for precision and throughput [1]. Inline measurements are consequently considered as a key factor for future industrial production [2], as they enable a 100 % quality control [3]. This would allow for realtime optimization of the manufacturing process and production parameter settings [4], [5], enhancing the overall throughput as well as the production yield.

Surface properties, such as topography and roughness, are frequently considered as quality indicators, which is why precise 3D measurements are of growing interest in application fields ranging from the semiconductor to the automotive and consumer electronics sector [6]–[9]. The flexibility to quickly align a 3D measurement tool (MT) to arbitrary locations on a freeform-shaped sample surface [10] and to extend its measurement range [11] can be provided by employing industrial robots. Current robot-based 3D imaging systems incorporate e.g. optical line sensors on a linear rail [12], [13] or stereo vision systems, both achieving resolutions down to 50 µm. However, the limited positioning accuracy of modern industrial robots, which is in the range of several tens of micrometers [14], makes robots themselves unsuitable for 3D surface measurements with single- or even sub-micrometer resolution [15].

Similar to the positioning uncertainty of robots, environmental vibrations in an industrial production line may cause relative motion between the MT and the sample surface, corrupting 3D measurements on the micrometer scale due to motion blur [16]. Considering these aspects, an inspection of each produced good with structural sizes in the single-micrometer range is usually not possible without impairing throughput, which is why typically sample-based inspections are conducted in a vibration-free lab environment.

In order to establish the required lab-like conditions for a conceptual precision 3D MT directly in the vibration-prone environment of an industrial production line, an active sample-tracking module aimed to act as a robot end-effector has been reported [17]. Since precision 3D MTs are typically rather bulky, a compact and lightweight scanning confocal chromatic sensor scanning confocal chromatic sensor (SCCS), targeted for robotic 3D measurement applications on a tracking module (TM) as an end-effector, has been proposed [18]. With concepts for the sub-components available, the integrated design of a precise robotic inline 3D measurement system with orientation-independent functionality is, however, still pending.

The contribution of this paper is i) the integrated system design of a robot-based inline measurement system for precise 3D surface inspection, and ii) the experimental validation of the orientation-independent 3D imaging performance in a vibrational environment. Focusing on the overall concept, a tailored TM with a sophisticated mechanical design is required for integration of the SCCS to proof the feasibility of robotic 3D measurements with sub-micrometer resolution.

II. Integrated measurement system design

The targeted system concept of precise robotic inline 3D measurements on freeforms is illustrated in Fig. 1. By main-

Manuscript received Month xx, 2xxx; revised Month xx, xxxx; accepted Month x, xxxx. This project is partially funded by the Hochschuljubilaeumsfonds of the city of Vienna, Austria under the project number H-260744/2020. The financial support by the Christian Doppler Research Association, the Austrian Federal Ministry for Digital and Economic Affairs, and the National Foundation for Research, Technology and Development, as well as MICRO-EPSILON MESSTECHNIK GmbH & Co. KG and ATENSOR Engineering and Technology Systems GmbH is gratefully acknowledged. The authors are with the Christian Doppler Laboratory for Precision Engineering for Automated In-Line Metrology, Automation and Control Institute (ACIN), Technische Universität Wien, 1040 Vienna. Corresponding author: wertjanz@acin.tuwien.ac.at

Post-print version of the article: D. Wertjanz, E. Csencsics, T. Kern, and G. Schitter, "Bringing the lab to the fab: Robot-based inline measurement system for precise 3D surface inspection in vibrational environments,"*IEEE/TIE* (Early Access Article), 2022. DOI: 10.1109/TIE.2022.3151959

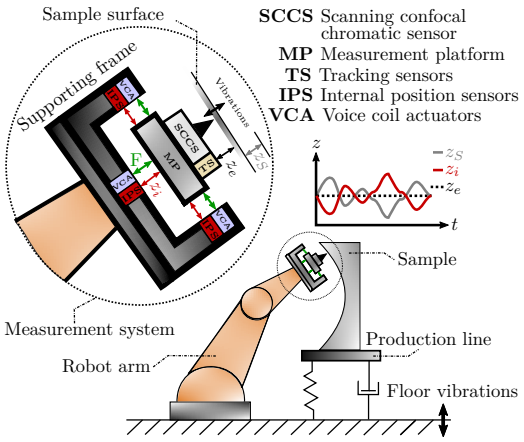

Fig. 1: Integrated robot-based measurement system for precise 3D surface inspection of freeform objects in vibrational environments. By means of feedback control, the position of the MT on the MP relative to the freeform surface is maintained constant.

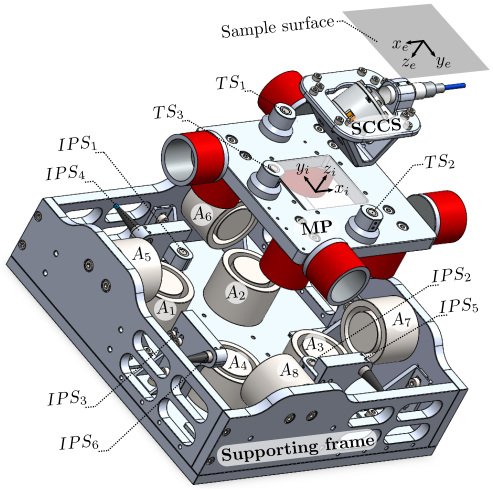

Fig. 2: Exploded view of the tracking module CAD model. VCAs are used for actuation of the MP in six DoFs. The SCCS is embedded in the MP. IPSs determine the position of the MP with respect to the supporting frame, while three TSs measure the external out-of-plane position and orientation relative to a sample surface.

taining a constant relative position of the measurement platform (MP) with respect to the sample surface, a contactless stiff link between the SCCS as a 3D MT and the surface area to be inspected is generated. In this way, the required lab-like conditions are established directly in a vibration-prone production line.

Figure 2 presents the novel integrated measurement system design, which comprises two main components, the TM to actively compensate disturbing vibrations and the SCCS to perform precision 3D measurements. The embedded electromagnetically levitated and actuated MP is tailored for the integration of the SCCS [18]. An actuation system (AS) based on voice coil actuators (VCAs) is used to achieve quasi-zero-stiffness actuation and thus, decoupling the MP from any external disturbances, such as vibrations from the robot. Eight identical VCAs A_1-A_8 are integrated to apply bi-directional forces, yielding a balanced MP design for the six degree of freedom (DoF) motion control. Waiving for a passive gravity compensation mechanism enables orientation-independent system operability [19], as required for the targeted robotic measurements on free-form surfaces. Since a lightweight moving mass is desired, the coils of the VCAs are mounted on the MP, which is actuated within the air gaps between coils and magnet assemblies. The achievable actuation range of the MP is strongly dependent on these air gaps, as well as the placement of the VCAs. Therefore, a design trade-off between achievable actuation range and levers of torque is required, with the chosen design parameters discussed in Section IV. As depicted in Fig. 2, the out-of-plane DoFs z, ϕ_x and ϕ_y are actuated by A_1-A_4, while A_5-A_8 enable in-plane positioning (x, y and ϕ_z) of the mover. In order to achieve a balanced system design and to minimize unintended crosstalk between the individual DoFs, the actuators are symmetrically placed beneath and around the center of mass of the moving part, i.e. MP with integrated SCCS.

Six internal position sensors (IPSs) are integrated to measure the MP position in all DoFs with respect to the supporting frame. The distance sensors IPS_4-IPS_6 are placed around the MP to measure its in-plane position (x_i, y_i and $\phi_{z,i}$), while IPS_1-IPS_3 are mounted beneath the MP to measure the out-of-plane position (z_i, $\phi_{x,i}$ and $\phi_{y,i}$).

In addition, the TM in Fig. 2 comprises three tracking sensors (TSs) TS_1-TS_3 mounted on the MP to measure the external out-of-plane position of the MP relative to a sample surface (z_e, $\phi_{x,e}$ and $\phi_{y,e}$). Considering the concept presented in Fig. 1, the system design of the TM is capable of actively compensating disturbing vibrations in the three out-of-plane DoFs, while generating quasi-lab conditions for the precision 3D measurements with the SCCS.

III. System Modeling

The decoupling between in- and out-of-plane actuation is achieved by the actuator placement discussed in Section II and shown in Fig. 2. Low crosstalk between the individual DoFs is ensured by a balanced system design and therefore neglected in the modeling phase, but analyzed in Section V-A. In order to ensure a constant current-to-force relation (quasi-zero-stiffness actuation), the hysteresis-free VCAs are operated around the MP's mid-position [20]. The ability of VCAs to apply bi-directional forces enables the required gravity compensation of the moving mass by orientation-dependent offset currents.

The TM dynamics for the MP's internal position $\zeta_\mathbf{i}$ relative to the supporting frame and the external position $\zeta_\mathbf{e}$ relative

Post-print version of the article: D. Wertjanz, E. Csencsics, T. Kern, and G. Schitter, "Bringing the lab to the fab: Robot-based inline measurement system for precise 3D surface inspection in vibrational environments,"*IEEE/TIE* (Early Access Article), 2022. DOI: 10.1109/TIE.2022.3151959

to a sample surface are

$$\begin{bmatrix}\ddot{\zeta}_{\mathbf{i,oop}}\\ \ddot{\zeta}_{\mathbf{i,ip}}\end{bmatrix} = \mathbf{Ai} = \begin{bmatrix}\mathbf{A_{oop}} & \mathbf{0_{3,3}}\\ \mathbf{0_{3,3}} & \mathbf{A_{ip}}\end{bmatrix}\begin{bmatrix}\mathbf{i_{oop}}\\ \mathbf{i_{ip}}\end{bmatrix} \tag{1a}$$

$$\begin{bmatrix}\zeta_{\mathbf{i,oop}}\\ \zeta_{\mathbf{i,ip}}\end{bmatrix} = \begin{bmatrix}\mathbf{h_{i,oop}}\left(\mathbf{d_{IPS,oop}}\right)\\ \mathbf{h_{i,ip}}\left(\mathbf{d_{IPS,ip}}\right)\end{bmatrix} \tag{1b}$$

$$\zeta_{\mathbf{e,oop}} = \mathbf{h_{e,oop}}\left(\mathbf{d_{TS,oop}}\right), \tag{1c}$$

with $\zeta_{\mathbf{i,oop}} = \begin{bmatrix} z_i & \phi_{x,i} & \phi_{y,i}\end{bmatrix}^T$ and $\zeta_{\mathbf{i,ip}} = \begin{bmatrix} x_i & y_i & \phi_{z,i}\end{bmatrix}^T$ the out-of- and in-plane MP position, $\mathbf{A_{oop}}$ and $\mathbf{A_{ip}}$ the according dynamic sub-matrices, and $\mathbf{i_{oop}} = \begin{bmatrix} i_z & i_{\phi_x} & i_{\phi_y}\end{bmatrix}^T$ and $\mathbf{i_{ip}} = \begin{bmatrix} i_x & i_y & i_{\phi_z}\end{bmatrix}^T$ being the in- and out-of-plane current vectors [17]. Trigonometric functions, $\mathbf{h_{i,oop}}$ and $\mathbf{h_{i,oop}}$, are applied to transform the measured out-of-plane and in-plane distances $\mathbf{d_{IPS,oop}} = [d_{IPS,1}, d_{IPS,2}, d_{IPS,3}]$ and $\mathbf{d_{IPS,ip}} = [d_{IPS,4}, d_{IPS,5}, d_{IPS,6}]$ into the actual MP's position $\zeta_\mathbf{i}$ with respect to the supporting frame (internal position). A similar transformation $\mathbf{h_{e,oop}}$ is applied to the distances $\mathbf{d_{TS,oop}} = [d_{TS,1}, d_{TS,2}, d_{TS,3}]$, measured by the three TSs, in order to calculate the MP's position $\zeta_\mathbf{e}$ relative to a sample surface (external position). Considering the two coordinate systems in Fig. 2, the dynamics of $\zeta_\mathbf{i}$ and $\zeta_\mathbf{e}$ are the same except for the sign, yielding

$$\dot{\zeta}_{\mathbf{e,oop}} = \dot{\mathbf{h}}_{\mathbf{e,oop}}\left(\mathbf{d_{TS,oop}}\right) = -\dot{\zeta}_{\mathbf{i,oop}}. \tag{2}$$

Assuming quasi-zero-stiffness actuation, the dynamic matrix from Eq. 1a

$$\mathbf{A} = \begin{bmatrix} \frac{4k_m}{m} & 0 & 0 & 0 & 0 & 0\\ 0 & \frac{4k_m l_x}{I_x} & 0 & 0 & 0 & 0\\ 0 & 0 & \frac{4k_m l_y}{I_y} & 0 & 0 & 0\\ 0 & 0 & 0 & \frac{2k_m}{m} & 0 & 0\\ 0 & 0 & 0 & 0 & \frac{2k_m}{m} & 0\\ 0 & 0 & 0 & 0 & 0 & \frac{4k_m l_z}{I_z}\end{bmatrix} \tag{3}$$

has only entries on the main diagonal, with m the total moving mass, k_m the VCA motor constant, l_x, l_y and l_z the levers of torque and I_x, I_y and I_z indicating the according moments of inertia in the rotational DoFs.

A linear transformation $\mathbf{i_a} = \mathbf{Ti}$ with the transformation matrix

$$\mathbf{T} = \begin{bmatrix}\mathbf{T_{oop}} & \mathbf{0_{4,3}}\\ \mathbf{0_{4,3}} & \mathbf{T_{ip}}\end{bmatrix} = \begin{bmatrix} 1 & 1 & 1 & 0 & 0 & 0\\ 1 & 1 & -1 & 0 & 0 & 0\\ 1 & -1 & -1 & 0 & 0 & 0\\ 1 & -1 & 1 & 0 & 0 & 0\\ 0 & 0 & 0 & 1 & 0 & -1\\ 0 & 0 & 0 & 0 & -1 & -1\\ 0 & 0 & 0 & -1 & 0 & -1\\ 0 & 0 & 0 & 0 & 1 & -1\end{bmatrix} \tag{4}$$

is applied to map the six currents from the vector $\mathbf{i}$ onto the individual currents $\mathbf{i_a} = \begin{bmatrix} i_1 & i_2 & i_3 & i_4 & i_5 & i_6 & i_7 & i_8\end{bmatrix}^T$ applicable to the eight VCA coils.

IV. System Implementation

Based on the integrated measurement system design from Section II, the individual system components are implemented with the design trade-offs discussed in detail in the following.

TABLE I: Design parameters of the implemented TM.

Parameter	Value	Description
k_m	$12.7\,\mathrm{N\,A^{-1}}$	VCA motor constant
m	890 g	Levitated and moving mass
l	50 mm	Lever of torque ϕ_x, ϕ_y, ϕ_z
I_x	1.47 mm kg	Moment of inertia ϕ_x
I_y	1.482 mm kg	Moment of inertia ϕ_y
I_z	2.74 mm kg	Moment of inertia ϕ_z

A. Mechanical components

All mechanical parts of the TM are manufactured out of aluminum to achieve the targeted stiff system and shift first structural modes to high frequencies. According to conducted FEM simulations, the first structural mode of the MP is excited at about 1.9 kHz (data not shown). The assembled system measures $220 \times 220 \times 72\,\mathrm{mm}^3$ in size and the total weight is about 5.25 kg. The supporting frame provides mounting holes for the magnet housings of the VCAs as well as brackets for the six IPSs. In the 10 mm thick and square MP with a side length of 125 mm a mounting hole for the SCCS is included. In addition, the coils of the VCAs can be mounted to the MP and brackets for the three TSs are provided. The total mass m of the assembled MP which needs to be levitated and actuated is about 890 g.

B. Actuation system

Eight conventional VCAs (VCAR0087-0062-00A, Supt-Motion, Suzhou, China) are selected to apply bi-directional forces to the MP and to enable the target orientation-independent operability of the TM. Each VCA shows an air gap of 500 µm and can provide 20 N continuous force. Considering the aforementioned design trade-off between applicable torque and achievable rotational actuation range, all levers of torque $l_x = l_y = l_z = l$ are chosen to 50 mm. With the MP in its center position, the implemented TM achieves an actuation range of about ±175 µm and ±3 mrad in the translational and rotational DoFs. The design parameters from the dynamic matrix in Eq. 3 are summarized in Tab. I. Based on the high-power operational amplifier OPA541 (Texas Instruments, Dallas, Texas, United States), custom-made analog proportional-integral (PI) voltage-controlled current controllers are implemented to apply the desired currents to the VCAs of the MP and the fast steering mirror (FSM) of the SCCS. The bandwidth of each analog current control loop (see $\mathbf{i_a}(\mathbf{u_{a,r}})$ and $\mathbf{i_b}(\mathbf{u_{b,r}})$ in Fig. 3b) is set to 15 kHz to avoid phase lag in the position control loops.

C. Internal position and tracking sensors

Capacitive displacement sensors (CSH05, Micro-Epsilon, Ortenburg, Germany) are used to measure the six distances $\mathbf{d_{IPS}}$ between supporting frame and MP and the three distances $\mathbf{d_{TS}}$ between MP and sample surface. Each of the nine sensor channels shows a measurement range of 500 µm with a constant gain of $50\,\mu\mathrm{m\,V^{-1}}$. After applying the nonlinear transformations in Eq. 1b and 1c to calculate the internal and external position of the MP, a position noise of 17 nm rms and 400 nrad rms for each translational and rotational DoF is achieved, respectively.

Post-print version of the article: D. Wertjanz, E. Csencsics, T. Kern, and G. Schitter, "Bringing the lab to the fab: Robot-based inline measurement system for precise 3D surface inspection in vibrational environments,"*IEEE/TIE* (Early Access Article), 2022. DOI: 10.1109/TIE.2022.3151959

D. Scanning confocal chromatic sensor for 3D imaging

The integrated design of the SCCS [18] includes a high performance 2D FSM [21] to manipulate the optical path of a high precision 1D confocal chromatic sensor (CCS) (IFS2404-2, Micro-Epsilon, Ortenburg, Germany). A multi-input-multi-output (MIMO) H_∞ controller C_{FSM} for the FSM axes is implemented to enable quick and precise scanning of the CCS's measurement spot across the surface area of interest. A data-driven image reconstruction procedure is implemented combining the FSM deflection angles and the correspondingly measured distances to the sample surface, in order to obtain an accurate 3D surface image. The SCCS can measure a volume of $0.35 \times 0.25 \times 1.8\,\mathrm{mm}^3$ with frame rates of up to 1 fps. Moreover, high resolution scans of arbitrary regions of interests (RoIs) can be performed with a lateral and axial resolution is of $2.5\,\mu\mathrm{m}$ and $76\,\mathrm{nm}$, respectively. Using the holes provided by the SCCS's aluminum alignment frame, the 3D MT is mounted to the MP (see Fig. 2) such that the measuring mid-range of the SCCS coincides with the mid-range of the capacitive TSs, which is about $250\,\mu\mathrm{m}$ in z-direction. A more detailed description of the compact SCCS enabling precision 3D measurements can be found in [18].

E. Rapid prototyping systems

High sampling rates are desired for the system in- and outputs to avoid phase lag and enable a high performance control of the MP position as well as performing precise scans with the FSM. Therefore, both digital position controllers in Fig. 3b, $\mathbf{C_{MP}}$ and $\mathbf{C_{FSM}}$, are implemented on a dSPACE MicroLabBox (MicroLabBox, dSPACE GmbH, Paderborn, Germany). To acquire the CCS's sensing signal and the actual angular deflection of the FSM, an industrial DAQ system (EK1100 and EL3702, Beckhoff Automation GmbH & Co. KG, Verl, Germany) is used. After acquisition of an entire measurement set, the synchronized data is applied to the image reconstruction procedure to obtain the desired 3D image. Both rapid prototyping systems operate at a sampling frequency of $40\,\mathrm{kHz}$.

F. System architecture

Based on the system design presented in Fig. 2, the TM is implemented and mounted to an industrial robot arm (KR10-2 R900, KUKA, Augsburg, Germany), as depicted in Fig. 3a.

Figure 3b represents the architecture of the individual system components in a schematic block diagram. Based on a cross-fading error gain (CFEG) [22], the MP can either be positioned relative to the supporting frame in six DoFs when the robot is repositioning (stabilization mode) or actively track a sample surface in the out-of-plane DoFs (tracking mode). The actual MP positioning error $\mathbf{e}_\zeta$ is applied to the position controller $\mathbf{C_{PID}}$ and the reference voltages $\mathbf{u_{a,r}}$ for the voltage-controlled current amplifiers $\mathbf{i_a}(\mathbf{u_{a,r}})$ are calculated using the linear transformation matrix $\mathbf{T}$ from Eq 4. The desired currents $\mathbf{i_a}$ are applied to the VCAs and the actual MP position is calculated by applying the distances measured by the IPS and TS system to Eq. 1b and 1c.

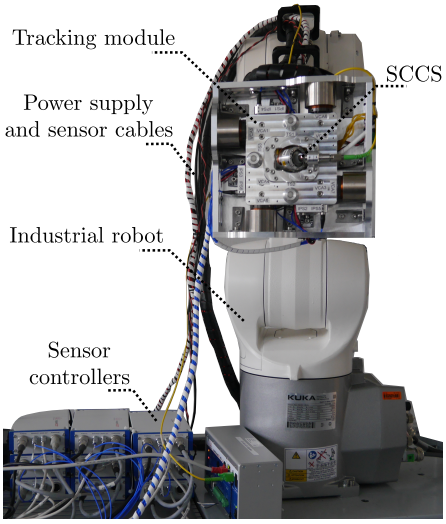

(a) Implemented TM mounted on an industrial robot arm.

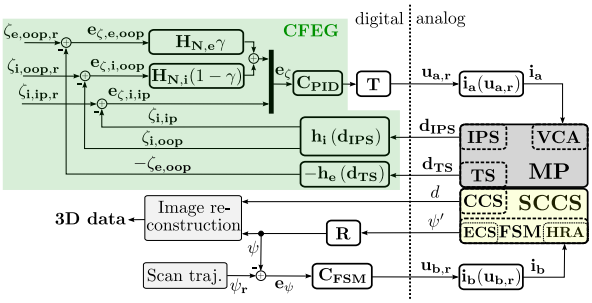

(b) Schematic block diagram.

Fig. 3: System implementation. a) depicts the lab setup with the integrated TM mounted on a robot. The schematic block diagram in b) illustrates the architecture of the individual system components.

To precisely deflect the FSM axes of the SCCS according to the desired scan trajectory, a high-performance motion controller $\mathbf{C_{FSM}}$ sets the reference voltage $\mathbf{u_{b,r}}$ for the voltage-controlled current amplifiers $\mathbf{i_b}(\mathbf{u_{b,r}})$. The output currents $\mathbf{i_b}$ are applied to the 2D hybrid-reluctance actuator (HRA) of the FSM. As the actuator and sensor axes of the FSM are rotated by 45°, the measured deflection ψ' by the integrated eddy current sensors (ECSs) is transformed using a rotation matrix $\mathbf{R}$ [18]. The actual FSM deflection ψ together with the distance d measured by the CCS, is applied to a calibration-based image reconstruction procedure which provides the targeted 3D data of the sample surface.

V. System Analysis and Control Design

The TM comprises two individual sensor systems to measure i) the internal MP position relative the supporting frame

Post-print version of the article: D. Wertjanz, E. Csencsics, T. Kern, and G. Schitter, "Bringing the lab to the fab: Robot-based inline measurement system for precise 3D surface inspection in vibrational environments,"*IEEE/TIE* (Early Access Article), 2022. DOI: 10.1109/TIE.2022.3151959

and ii) the external out-of-plane MP position relative to a sample surface. The internal and external TM dynamics measured with the IPSs and TSs, respectively, are analyzed in the following. Moreover, a control structure enabling the smooth transition between stabilization of the MP and the tracking of a sample surface, is presented.

A. Analysis of system dynamics

In a first step, the TM's internal dynamics are identified in closed-loop operation by means of low-bandwidth floating-mass model-based proportional-integral-derivative (PID) controller designed for each DoF to stabilize the MP in a free-floating position relative to the supporting frame. Sinusoidal sweeps with small amplitudes of 1 µm and 50 µrad are applied as reference for the low-bandwidth single-input single-output (SISO) controller of each translational and rotational DoF, respectively. By dividing the measured internal position signal by the according controller output, the individual internal system dynamics are obtained. Due to the balanced system design, the measured crosstalk between the individual DoFs for frequencies up to 1 kHz is 14 to 25 dB lower than the related system dynamics (data not shown). The dynamics analysis is exemplarily shown for DoF z in Fig. 4 and includes the time delay of the rapid prototyping system as well as the dynamics of the AS, the MP and IPS system. In the frequency range between 30 and 1.4 kHz, good agreement between the measured internal dynamics G_i and the floating mass model (FMM) G_{FMM} is achieved.

As given by Eq. 2, the internal and external out-of-plane MP dynamics show equal magnitude and a phase shift 180° (see [17]). By repeating the identification process in tracking control mode, the three external out-of-plane TM dynamics are identified. As expected and exemplarily shown in Fig. 4 for DoF z, the internal dynamics G_i match the 180° phase-shifted external dynamics G_e. Measured structural modes above 1.4 kHz are measured slightly different due to different mounting positions of IPS_1-IPS_3 and TS_1-TS_3 in the xy-plane (see Fig. 2).

B. Motion control

A SISO PID control approach for the two individual control tasks of the MP, i) the stabilization relative to the supporting frame and ii) the active tracking of a sample surface, is pursued as the measured crosstalk is sufficiently low [19]. For each internal and external DoF, tamed PID controllers

$$C_{PID} = k_p + \frac{k_i}{s} + \frac{k_d s}{1 + \frac{s}{\omega_t}} \tag{5}$$

are synthesized in a loop shaping approach aiming to maximize the positioning control bandwidth [23].

As previously discussed in Section V-A, the internal and external out-of-plane MP dynamics are similar, enabling the use of the same PID parameters for both control tasks, stabilization and tracking, by shifting the external position measured by 180° [22]. Excitation of the structural modes identified at frequencies beyond 1.4 kHz is suppressed by

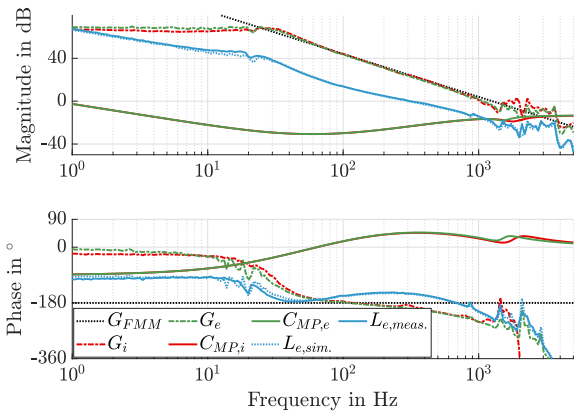

Fig. 4: Analysis of system dynamics and controller design of DoF z. The measured in- and external dynamics are in good accordance ($G_i \approx G_e$) and match the mathematical floating mass model G_{FMM}. The stabilization controller $C_{MP,i}$ and tracking controller $G_{MP,e}$ differ only by tailored notch filters at frequencies above 1.4 kHz.

TABLE II: Designed GMs and PMs of internal (stabilization) and external (tracking) position control loop gains.

	DoF	ω_c	GM	PM
stabilziation	z_i	340 Hz	9.8 dB	30.5°
	$\phi_{x,i}$	320 Hz	8.7 dB	31.8°
	$\phi_{y,i}$	320 Hz	8.8 dB	31.7°
	x_i	300 Hz	8.1 dB	29.8°
	y_i	300 Hz	8.3 dB	30.3°
	$\phi_{z,i}$	290 Hz	8.1 dB	27.9°
tracking	z_e	340 Hz	9.7 dB	30.4°
	$\phi_{x,e}$	320 Hz	8.1 dB	29.9°
	$\phi_{y,e}$	320 Hz	8.4 dB	29.1°

applying tailored notch filters $\mathbf{H_{N,k}}$, $k \in \{i, e\}$. The resulting combined structure of the MP motion controller

$$\mathbf{C_{MP,k}} = \mathbf{C_{PID}} \mathbf{H_{N,k}}, \; k \in \{i, e\} \tag{6}$$

is designed for each in- and external DoF with a crossover frequency of about 320 Hz. To ensure robustness, sufficient gain margin (GM) and phase margin (PM) of at least 8 dB and 25° for each DoF are targeted in the controller synthesis. A summary of the designed GMs and PMs at the desired crossover frequencies ω_c of the individual internal and external position control loops is listed in Tab. II.

In Fig. 4 the controllers designed for the two individual control tasks in DoF z are exemplarily shown. As can be seen, the controllers $C_{MP,i}$ and $C_{MP,e}$ differ only by the tailored and individually designed notch filters, applied at frequencies above 1.4 kHz to cancel the measured structural modes. Between the resulting simulated and measured loops gains of the external position, $L_{e,sim.}$ and $L_{e,meas.}$, good accordance is achieved. The crossover frequency of 340 Hz is clearly visible, together with the gain and phase margins of 9.8 dB and 30.5°.

Figure 5 shows the measured complementary sensitivities T and sensitivities S of the three out-of-plane DoFs in tracking

Post-print version of the article: D. Wertjanz, E. Csencsics, T. Kern, and G. Schitter, "Bringing the lab to the fab: Robot-based inline measurement system for precise 3D surface inspection in vibrational environments,"*IEEE/TIE* (Early Access Article), 2022. DOI: 10.1109/TIE.2022.3151959

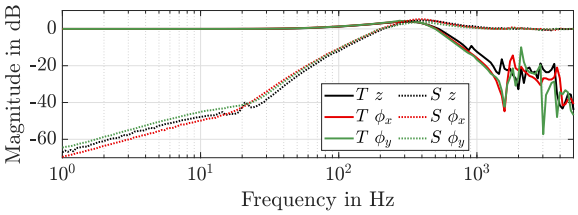

Fig. 5: Complementary sensitivity T and sensitivity S of the implemented 3 DoF tracking control. A $-3\,\mathrm{dB}$ tracking control bandwidth of about $600\,\mathrm{Hz}$ and good disturbance rejection at low frequencies are obtained.

mode, while the MP is stabilized in-plane relative to the supporting frame. A $-3\,\mathrm{dB}$ tracking control bandwidth of about $600\,\mathrm{Hz}$ is achieved in all three DoFs. According to the sensitivities (dotted lines), good disturbance rejection is obtained for lower frequencies, e.g. a vibration component with a frequency of $10\,\mathrm{Hz}$ can be attenuated by about $48\,\mathrm{dB}$ in DoF z, which equals a factor of about 250. An efficient transition between the stabilization and tracking mode is enabled by implementation of the CFEG-based control scheme from Fig. 3b [22].

VI. Experimental Performance Evaluation

A. Vibration compensation by active sample-tracking

In a first step, the vibration compensation of floor vibration spectra is demonstrated. Therefore, a randomized signal with $15.5\,\mu\mathrm{m\,rms}$ meeting the VC-A norm [24] is applied to a 1 DoF shaker, emulating standardized floor vibrations in DoF z. Using the industrial robot, the TM is aligned to the sample surface on the shaker. With the TM in stabilization mode, the relative motion between the SCCS and the sample surface is represented by the positioning error e of DoF z in grey in Fig. 6. Repeating the measurement for the same vibration signal with the TM in tracking mode, a residual error of only $236\,\mathrm{nm\,rms}$ is obtained (zoomed plot of Fig 6). Thus, the control-induced stiff link between the SCCS and the sample surface is capable of attenuating $98.5\,\%$ of the vibration-caused relative motion in DoF z.

B. Robot-based 3D imaging in vibrational environment

In order to evaluate the TM's 3D imaging performance in vibrational environments, a calibration standard with $20\,\mu\mathrm{m}$ pitch and step heights of $25\,\mu\mathrm{m}$ (Nanuler Calibration Standard, Applied NanoStructures Inc., Mountain view, CA, USA) is mounted to the 1-DoF shaker. 3D images of the sample surface are acquired by applying a Lissajous scan trajectory to the FSM with a total measurement time of $T = 10\,\mathrm{s}$. A reference measurement of the grating structure is conducted with enabled tracking control mode, but without applying vibrations to the shaker. The resulting reference image of the sample surface is shown in Fig. 7a, with the grating pitch of $20\,\mu\mathrm{m}$ measured correctly. The measured height z along the top of the grating at $x = 140\,\mu\mathrm{m}$ in Fig. 7b is evaluated to $571\,\mathrm{nm\,rms}$ and serves as a reference value. As the CCS's

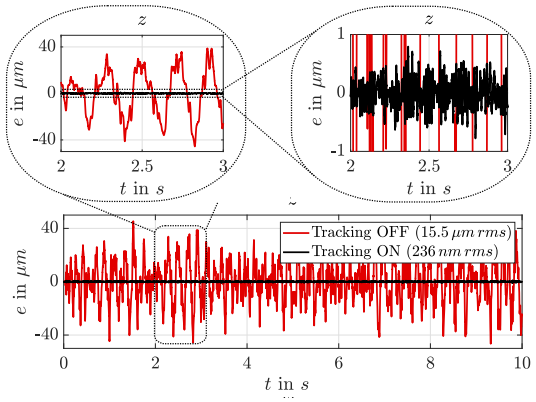

Fig. 6: Vibration compensation by active sample-tracking. With the TM in tacking mode (black), a $15.5\,\mu\mathrm{m\,rms}$ vibration signal (VC-A norm) is attenuated to a residual error of $236\,\mathrm{nm\,rms}$.

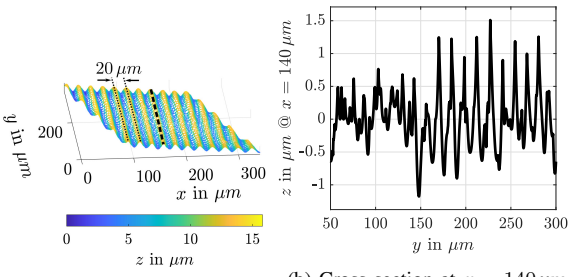

(a) Reference 3D image.

(b) Cross section at $x = 140\,\mu\mathrm{m}$.

Fig. 7: Reference measurement of the grating structure. a) The grating pitch of $20\,\mu\mathrm{m}$ is clearly visible. b) shows the measured z-ripple along the grating top at $x = 140\,\mu\mathrm{m}$.

light spot diameters equals the structural width ($10\,\mu\mathrm{m}$), the periodical peaks in Fig. 7b are most probably caused by light scattering at the sharp grating edges.

The 3D imaging capability of the TM in vibrational environment and different static robot poses is shown in Fig. 8. Using the robot arm, the TM is aligned to the 1-DoF shaker, on which the calibration standard with the $20\,\mu\mathrm{m}$ grating is mounted, such that the three TSs and the SCCS are in range. To demonstrate the systems orientation-independent operability, the system performance in horizontal and vertical orientation is investigated (see Fig. 8a and 8b).

Again, a vibration signal according to the VC-A norm is applied to the 1-DoF shaker, introducing relative motion between the SCCS and the sample surface. With the TM in stabilization mode, motion blur in the 3D measurements (see Fig.8c and 8d) is caused and the $20\,\mu\mathrm{m}$ grating structure is not visible. By enabling the tracking mode, the targeted contactless stiff link between SCCS and sample surface is established. The 3D measurements for the measurement system in tracking mode and the same vibration signal applied to the shaker are shown in Fig. 8e and 8f. The $20\,\mu\mathrm{m}$ grating pitch is

Post-print version of the article: D. Wertjanz, E. Csencsics, T. Kern, and G. Schitter, "Bringing the lab to the fab: Robot-based inline measurement system for precise 3D surface inspection in vibrational environments,"*IEEE/TIE* (Early Access Article), 2022. DOI: 10.1109/TIE.2022.3151959

clearly visible and measured correctly in both orientations. To quantify the measurement system performance, the cross sections at $x = 140\,\mu\text{m}$ in the 3D images, indicated in dashed black, is evaluated and shown in Fig. 8g and 8h for dis- and enabled tracking control, respectively. In both orientations, the measurement uncertainty is reduced from about $11\,\mu\text{m rms}$ to $900\,\text{nm rms}$, improving the 3D imaging performance by a factor of 12. Compared to the reference 3D measurement in Fig. 7, the imaging resolution is in the same order of magnitude.

In summary, the integrated robotic measurement system successfully enables precision 3D measurements on freeform surfaces with a resolution on the sub-micrometer scale, compensating for $98.5\,\%$ of disturbing vibrations in the translational out-of-plane DoF.

VII. Conclusion

This paper presents a measurement system for robotic precision 3D measurements on freeform surfaces in arbitrary orientations. The system design comprises a MAGLEV MP with three integrated TSs measuring the out-of-plane position of the SCCS as a 3D MT relative to a sample surface. In addition, six IPSs measure the MP position in six DoFs with respect to the supporting frame. Applying a SISO PID control architecture, the MP can track a sample surface while it is stabilized in-plane relative to the supporting frame. A positioning control bandwidth of about $600\,\text{Hz}$ is achieved for each DoF. Standardized floor vibration profiles are applied to a sample surface in order to evaluate the system performance. Experimental results demonstrate that $98.5\,\%$ of disturbing vibrations are actively compensated by the TM in the translational out-of-plane DoF. An industrial robot is used to position the TM in different orientations relative to a vibrating $20\,\mu\text{m}$ grating structure. By enabling the tracking control, the measurement uncertainty is improved by a factor of 12, enabling robot-based precision 3D measurements on freeform surfaces on the sub-micrometer scale in vibrational environments.

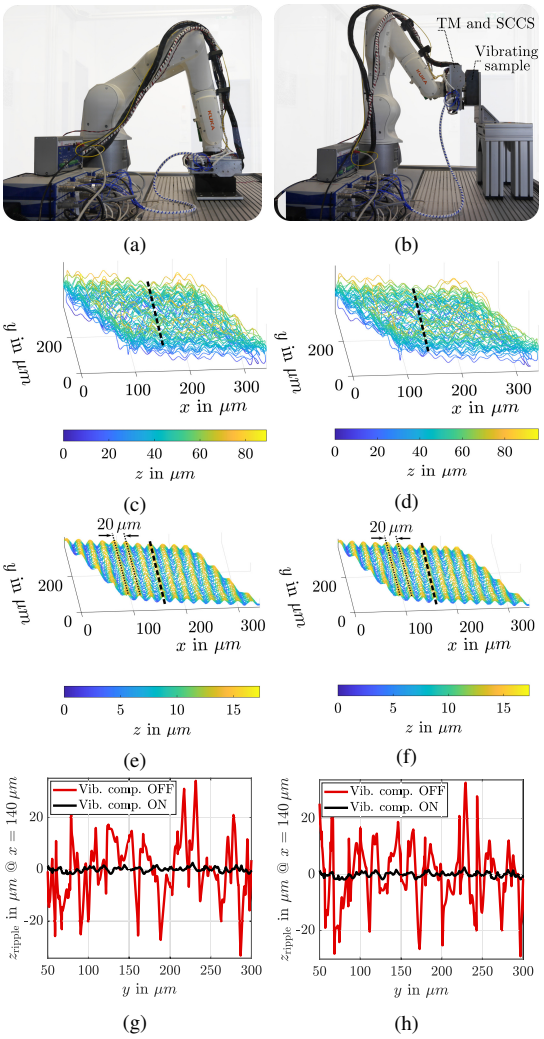

Fig. 8: Robot-based precision 3D imaging in vibrational environment. a) and b) show the measurement system positioned by the robot in horizontal and vertical direction. c) and d) illustrate blurry 3D images for disabled tracking control. e) and f) demonstrate the precise measurement of the grating structure with enabled out-of-plane tracking control. In g) and h), the measurement uncertainty along the cross section at $x = 140\,\mu\text{m}$ in the 3D measurements (dashed black line) is shown for enabled and disabled tracking mode.

References

[1] T. Uhrmann, T. Matthias, M. Wimplinger, J. Burggraf, D. Burgstaller, H. Wiesbauer, and P. Lindner, "Recent progress in thin wafer processing," in *2013 IEEE International 3D Systems Integration Conference (3DIC)*, pp. 1–8, 2013.

[2] D. Imkamp, R. Schmitt, and J. Berthold, "Blick in die Zukunft der Fertigungsmesstechnik - Die VDI/VDE-GMA Roadmap Fertigungsmesstechnik 2020." *Technisches Messen*, vol. 10, no. 79, 2012.

[3] R. Schmitt and F. Moenning, "Ensure success with inline-metrology," in *XVIII IMEKO World Congress - Metrology for a Sustainable Development*, 2006.

[4] W. Gao, H. Haitjema, F. Fang, R. Leach, C. Cheung, E. Savio, and J. Linares, "On-machine and in-process surface metrology for precision manufacturing," *CIRP Annals*, vol. 68, no. 2, pp. 843 – 866, 2019.

[5] M. Grasso and B. Colosimo, "Process defects and in situ monitoring methods in metal powder bed fusion: a review," *Measurement Science and Technology*, vol. 28, p. 044005, 2017.

[6] A. Yogeswaran and P. Payeur, "3d surface analysis for automated detection of deformations on automotive body panels," in *New Advances in Vehicular Technology and Automotive Engineering*. IntechOpen, 2012.

[7] "In-line dimensional metrology in nanomanufacturing systems enabled by a passive semiconductor wafer alignment mechanism," *Journal of Micro- and Nano-Manufacturing*, vol. 5, no. 1.

[8] G. Sansoni, M. Trebeschi, and F. Docchio, "State-of-the-art and applications of 3d imaging sensors in industry, cultural heritage, medicine, and criminal investigation," *Sensors (Basel, Switzerland)*, vol. 9, pp. 568–601, 01 2009.

[9] H. Schwenke, U. Neuschaefer-Rube, T. Pfeifer, and H. Kunzmann, "Optical methods for dimensional metrology in production engineering," *CIRP Annals*, vol. 51, no. 2, pp. 685–699, 2002.

[10] E. Savio, L. D. Chiffre, and R. Schmitt, "Metrology of freeform shaped parts," *CIRP Annals*, vol. 56, no. 2, pp. 810 – 835, 2007.

[11] J. Rejc, J. Cinkelj, and M. Munih, "Dimensional measurements of a gray-iron object using a robot and a laser displacement sensor," *Robotics and Computer-Integrated Manufacturing*, vol. 25(1), pp. 155–167, 2009.

Post-print version of the article: D. Wertjanz, E. Csencsics, T. Kern, and G. Schitter, "Bringing the lab to the fab: Robot-based inline measurement system for precise 3D surface inspection in vibrational environments,"*IEEE/TIE* (Early Access Article), 2022. DOI: 10.1109/TIE.2022.3151959

[12] S. Yin, Y. Ren, Y. Guo, J. Zhu, S. Yang, and S. Ye, "Development and calibration of an integrated 3d scanning system for high-accuracy large-scale metrology," *Measurement*, vol. 54, pp. 65–76, 2014.
[13] G. B. de Sousa, A. Olabi, J. Palos, and O. Gibaru, "3d metrology using a collaborative robot with a laser triangulation sensor," *Procedia Manufacturing*, vol. 11, pp. 132–140, 2017.
[14] U. Schneider, M. Drust, M. Ansaloni, C. Lehmann, M. Pellicciari, F. Leali, J. Gunnink, and A. Verl, "Improving robotic machining accuracy through experimental error investigation and modular compensation," *The International Journal of Advanced Manufacturing Technology*, vol. 85, pp. 1–13, 06 2014.
[15] E. Csencsics, M. Thier, S. Ito, and G. Schitter, "Supplemental peak filters for advanced disturbance rejection on a high precision endeffector for robot-based inline metrology," *IEEE/ASME Transactions on Mechatronics (Early Access)*, 2021.
[16] R. Saathof, M. Thier, R. Hainisch, and G. Schitter, "Integrated system and control design of a one dof nano-metrology platform," *Mechatronics*, vol. 47, pp. 88 – 96, 2017.
[17] D. Wertjanz, E. Csencsics, and G. Schitter, "3 dof vibration compensation platform for robot-based precision inline measurements on free-form surfaces," *IEEE Transactions on Industrial Electronics (Early Access)*, 2021.
[18] D. Wertjanz, T. Kern, E. Csencsics, G. Stadler, and G. Schitter, "Compact scanning confocal chromatic sensor enabling precision 3-d measurements," *Appl. Opt.*, vol. 60, no. 25, pp. 7511–7517, Sep. 2021.
[19] D. Wertjanz, E. Csencsics, J. Schlarp, and G. Schitter, "Design and control of a maglev platform for positioning in arbitrary orientations," in *2020 IEEE/ASME International Conference on Advanced Intelligent Mechatronics (AIM)*, pp. 1935–1942, 2020.
[20] S. Ito, D. Neyer, S. Pirker, J. Steininger, and G. Schitter, "Atomic force microscopy using voice coil actuators for vibration isolation," *2015 IEEE International Conference on Advanced Intelligent Mechatronics (AIM)*, pp. 470–475, 2015.
[21] E. Csencsics, J. Schlarp, T. Schopf, and G. Schitter, "Compact high performance hybrid reluctance actuated fast steering mirror system," *Mechatronics*, vol. 62, no. March, p. 102251, 2019.
[22] D. Wertjanz, E. Csencsics, and G. Schitter, "An efficient control transition scheme between stabilization and tracking task of a maglev platform enabling active vibration compensation," in *2020 IEEE/ASME International Conference on Advanced Intelligent Mechatronics (AIM)*, pp. 1943–1948, 2020.
[23] E. Csencsics and G. Schitter, "Parametric pid controller tuning for a fast steering mirror," in *2017 IEEE Conference on Control Technology and Applications (CCTA)*, pp. 1673–1678, 2017.
[24] C. G. Gordon, *Generic Vibration Criteria for Vibration-Sensitive Equipment*, Colin Gordon & Associates, 1999.

Daniel Wertjanz is doctoral researcher at the Automation and Control Institute (ACIN) at TU Wien, Vienna, Austria. He received an MSc. degree in Electrical Engineering from TU Wien in 2019. His primary research interests are on high performance mechatronic systems design, high precision motion control, and automated inline measurement systems.

Ernst Csencsics is assistant professor for Metrology Systems in the Advanced Mechatronic Systems group at the Automation and Control Institute (ACIN) of TUWien. He received an MSc. and a PhD degree (sub auspiciis) in Electrical Engineering from TU Vienna, Austria in 2014 and 2017, respectively. His primary research interests are on high performance mechatronic systems, the development of holistic methods for multidisciplinary system design and integration, opto-mechatronic measurement and imaging systems, precision engineering, and robot-based in-line measurement systems. He received the journal best paper award of IEEE/ASME Transactions on Mechatronics (2018) and the best student paper award at the American Control Conference (2016).

Thomas Kern is researcher at the Automation and Control Institute (ACIN) at TU Wien, Vienna, Austria. He received a BSc. degree in Electrical Engineering from TU Wien in 2021. His primary research interests are on high precision motion control and advanced mechatronic systems.

Georg Schitter is Professor for Advanced Mechatronic Systems at the Automation and Control Institute (ACIN) of TU Wien. He received an MSc in Electrical Engineering from TU Graz, Austria (2000) and an MSc and PhD degree from ETH Zurich, Switzerland (2004). His primary research interests are on high-performance mechatronic systems, particularly for applications in the high-tech industry, scientific instrumentation, and mechatronic imaging systems, such as AFM, scanning laser and LIDAR systems, telescope systems, adaptive optics, and lithography systems for semiconductor industry. He received the journal best paper award of IEEE/ASME Transactions on Mechatronics (2018), of the IFAC Mechatronics (2008-2010), of the Asian Journal of Control (2004-2005), and the 2013 IFAC Mechatronics Young Researcher Award. He served as an Associate Editor for IFAC Mechatronics, Control Engineering Practice, and for the IEEE Transactions on Mechatronics.

Post-print version of the article: D. Wertjanz, E. Csencsics, T. Kern, and G. Schitter, "Bringing the lab to the fab: Robot-based inline measurement system for precise 3D surface inspection in vibrational environments,"*IEEE/TIE* (Early Access Article), 2022. DOI: 10.1109/TIE.2022.3151959